Mon. Not. R. Astron. Soc. **283,** 297–315 (1996)

Non-local thermodynamic equilibrium effects in modelling of supernovae near maximum light

E. Baron,[1] P. H. Hauschildt,[2] P. Nugent[1] and D. Branch[1]

[1]*Dept. of Physics and Astronomy, University of Oklahoma, 440 W. Brooks, Rm 131, Norman, OK 73019-0225*
[2]*Dept. of Physics and Astronomy, Arizona State University, Tempe, AZ 85287-1504*

Accepted 1996 July 1. Received 1996 May 20; in original form 1996 March 12

ABSTRACT

Supernovae (SNe), with their diversity of compositions, velocities, envelope masses, and interactions, are good testing grounds for probing the importance of non-local thermodynamic equilibrium (NLTE) in expanding atmospheres. In addition to treating H, He, Li I, O I, Ne I, Na I, and Mg II in NLTE, we use a very large model atom of Fe II to test the importance of NLTE processes in both Type Ia and Type II SNe. Since the total number of potential line transitions that one has to include is enormous ($\approx$ 40 million), approximations and simplifications are required to treat the problem accurately and in finite computer time. With our large Fe II model atom (617 levels and 13 675 primary NLTE line transitions) we are able to test several assumptions for treating the background opacity that are needed to obtain correct UV line blanketing, which determines the shape of near-maximum light supernova spectra. We find that, due to interactions within the multiplets, treating the background lines as pure scattering (thermalization parameter $\varepsilon = 0$) is a poor approximation, and that an overall mean value of $\varepsilon \sim 0.05$–0.10 is a far better approximation. This is true even in SNe Ia, where the continuum absorption optical depth at 5000 Å ($\equiv \tau_{\rm std}$) is $\ll 1$. We also demonstrate that a detailed treatment of NLTE effects is required to determine properly the ionization states of both abundant and trace elements.

Key words: radiative transfer – stars: atmospheres – stars: evolution – supernovae: general.

1 INTRODUCTION

Modelling the light curve and spectrum of a supernova is in principle a daunting task, since it requires full NLTE radiation hydrodynamics in three spatial dimensions and a detailed understanding of the explosion mechanism. The dynamic range and computing capacity required for such detailed modelling do not currently exist. In practice, one can do spherically symmetric LTE multi-group radiation hydrodynamics (e.g. Höflich 1995) to determine the light curve, or one can calculate steady-state detailed model atmospheres (e.g. Baron et al. 1995; Nugent et al. 1995). In fact, until details of the explosion mechanisms are worked out and one gains the ability to account for complicated micro- and macroscopic mixing, these approaches are both reasonable and accurate enough to extend our understanding of the nature and systematics of SNe, although in principle one would like to relax the LTE assumption in the light curve models. Even within this somewhat limited framework, treating all 40 million radiative transitions that occur in detailed NLTE is beyond the capability of presently available computers, and there is always the caveat that the atomic data is likely to be inaccurate for many transitions. Nevertheless, through the use of a non-local approximate lambda operator we have been able to include (on workstation-class computers) very detailed model atoms of iron group elements (Hauschildt 1992, 1993; Hauschildt & Baron 1995). Our aim in this paper is to examine the effects of using such model atoms on the synthetic spectra of both type Ia (SN Ia) and type II (SN II) supernovae and to use the knowledge gained from numerical experiments to guide our necessarily approximate treatment of the additional million or so radiative rates that are required to correctly reproduce the UV line blanketing that occurs in SNe near

maximum light. Actually, the task is even more difficult: while including about 500 000 lines saturates the opacity, and the overall spectral shape and detailed line-shapes are well reproduced, which 500 000 transitions are the most important varies with supernova and phase and therefore must be dynamically determined from the full list of 40 million possible transitions.

We briefly describe the Fe II model atom and the basic features of supernova model atmospheres (details can be found in Baron et al. 1995; Nugent et al. 1995; Hauschildt & Baron 1995). Some of the description of the methods in Section 2 and 3 has appeared in a companion paper on novae (Hauschildt et al. 1996), although the details are presented in those sections for supernova models as opposed to nova models. The reader familiar with Hauschildt et al. (1996) may wish to examine the figures in those sections and then skip to Section 4, in which we discuss results we have obtained for representative supernova model atmospheres. We conclude with a summary and discussion.

2 METHODS AND MODELS

2.1 Radiative transfer

In the Lagrangian frame ('comoving frame'), the special relativistic equation of radiative transfer is given by (e.g. Mihalas & Mihalas 1984)

$$\gamma(\mu+\beta)\frac{\partial I}{\partial r}+\frac{\partial}{\partial \mu}\left\{\gamma(1-\mu^2)\left[\frac{(1+\beta\mu)}{r}-\gamma^2(\mu+\beta)\frac{\partial \beta}{\partial r}\right]I\right\}$$

$$-\frac{\partial}{\partial \nu}\left\{\gamma\left[\frac{\beta(1-\mu^2)}{r}+\gamma^2\mu(\mu+\beta)\frac{\partial \beta}{\partial r}\right]\nu I\right\}$$

$$+\gamma\left[\frac{2\mu+\beta(3-\mu^2)}{r}+\gamma^2(1+\mu^2+2\beta\mu)\frac{\partial \beta}{\partial r}\right]I$$

$$=\tilde{\eta}-\chi I. \qquad (1)$$

Here, r is the radius, μ the cosine of the angle between a ray and the direction normal to the surface, ν the frequency, $I=I(r,\mu,\nu)$ denotes the specific intensity at radius r and frequency ν in the direction $\arccos(\mu)$ in the Lagrangian frame. The matter velocity $v(r)$ is measured in units of the speed of light c: $\beta(r)=v(r)/c$ and γ is given by $\gamma(r)=1/\sqrt{1-\beta^2}$. The sources of radiation present in the matter are described by the emission coefficient $\tilde{\eta}=\tilde{\eta}(r,\nu)$, and $\chi=\chi(r,\nu)$ is the extinction coefficient.

We solve equation (1) using an operator-splitting method with an exact non-local band-matrix approximate Λ-operator (Hauschildt 1992; Hauschildt, Störzer & Baron 1994). We can safely neglect the *explicit* time dependencies and *partial* time derivatives $\partial/\partial t$ in the radiative transfer because the radiation-flow timescale is much smaller than the timescale of the evolution of the SNe outburst (at least near maximum light). However, the advection and aberration terms must be retained in order to obtain a physically consistent solution (Mihalas & Mihalas 1984; Peraiah 1987, 1991a,b). This approach is also consistent with the equation of radiation hydrodynamics in the time-independent limit (Mihalas & Mihalas 1984; Baron, Hauschildt & Mezzacappa 1996a). We neither neglect the Lagrangian time derivative $\mathrm{D}/\mathrm{D}t=\partial/\partial t+v\partial/\partial r$, nor assign an ad hoc value to $\mathrm{D}/\mathrm{D}t$ (Eastman & Pinto 1993). The latter two assumptions lead to physical inconsistencies with the equations of radiation hydrodynamics (e.g. they do not lead to the correct equations for a steady-state stellar wind). Our approach is physically self-consistent because it includes the important advection and aberration terms in both the non-grey radiative transfer and the radiative energy equations. The *only* term that we neglect is the *explicit* time dependence, which is a very good approximation in nova and supernova atmospheres (Baron et al. 1996a).

Although our method is much more complicated than using ad hoc assumptions for $\mathrm{D}/\mathrm{D}t$ (because of the additional terms in the equations that must be handled that break the symmetry of the characteristics of the radiative transfer equation), its results are much more reliable than those of simpler methods. In addition, the solution of the correct set of radiative transfer and energy equations in the comoving frame is no more time consuming that the solution of the corresponding static problem. This is because of our use of a non-local approximate Λ-operator.

2.2 Treatment of spectral lines

The physical conditions prevailing in nova and supernova atmospheres are such that a large number of spectral lines are present in the line-forming regions. Therefore, the simple Sobolev approximation *cannot* be used for accurate modelling including both line and continuum transfer, because many lines of comparable strength overlap (see Hauschildt et al. 1995). This means that the basic assumptions required to derive the Sobolev approximation are not valid. We demonstrate this in Fig. 1 in which we plot the number of lines that are stronger than the local bound–free (b–f) continuum and that lie within a ± 2 Doppler-width wavelength interval around each wavelength point in the comoving frame. This graph is for a representative SN Ia atmosphere [W7 abundances (Nomoto, Thielemann & Yokoi 1984), homogenized for $v>8000$ km s^{-1}, see e.g. Nugent et al. (1995)] with an effective temperature of 9000 K, and a microturbulent or statistical velocity of $\xi=2$ km s^{-1}. In the UV, the number of overlapping strong lines at each wavelength point is typically larger than 100; in some regions as many as 300 strong lines lie within 2 Doppler-widths. Even in some regions of the optical spectral range, the number of overlapping lines can be as high as 200 or more. Fig. 1 shows that the situation becomes much worse for weaker lines (lines that are stronger than 10^{-3} of the local b–f continuum must be included in supernova atmosphere models). Now, nearly 1000 lines (all of comparable strength) overlap in the UV and around 300 lines in the optical can overlap at each wavelength point. This shows decisively that the Sobolev approximation cannot be used in modelling supernova atmospheres. In light of this observation, our approach solves the full radiative transfer equation for all lines. In addition, we wish to model stellar atmospheres (both static cool stars, and hot stars with winds), and in those case the Sobolev approximation does not apply.

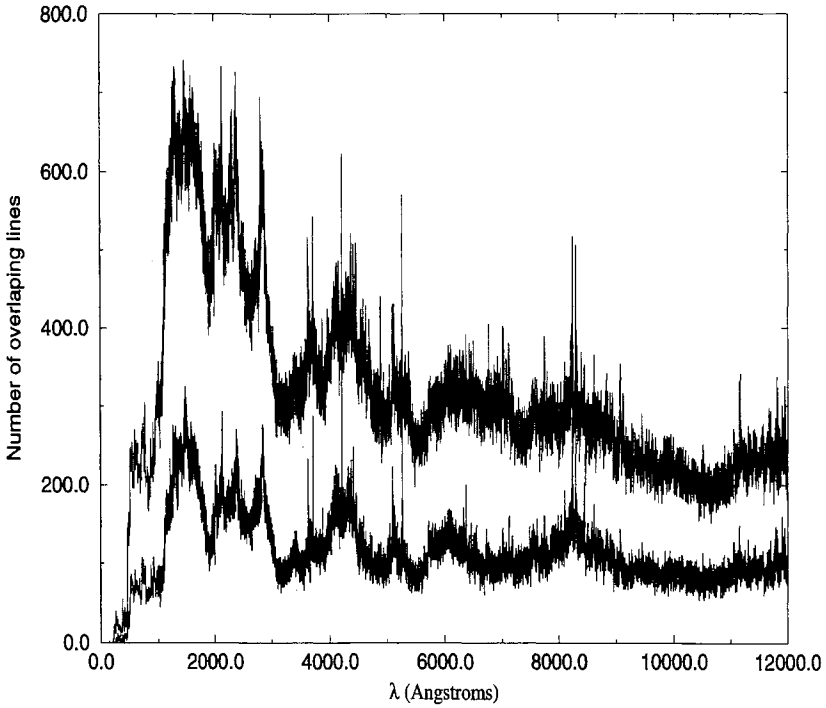

Figure 1. The lower line shows the number of overlapping lines within two Doppler widths of each wavelength point when lines are included that are at least as strong as the bound–free continuum. The upper line shows the same when weak lines that are within 0.01 of the bound–free continuum are included.

3 THE FE II MODEL ATOM

We have taken the data needed to construct our model atom from the compilation of Kurucz (1994), whose long term project to provide accurate atomic data for modelling stellar atmospheres is an invaluable service to the scientific community. For our current model atom, we have kept terms up to the ^{2}H term, which corresponds to the first 29 terms of Fe II. Within these terms, we include all observed levels that have observed bound–bound (b–b) transitions with $\log gf > -3.0$ as NLTE levels (where g is the statistical weight of the lower level and f is the oscillator strength of the transition). This leads to a model atom with 617 levels and 13 675 'primary' transitions, which we treat in detailed NLTE. We solve the complete b–f and b–b radiative transfer and rate equations for all these levels and include all radiative rates of the primary lines. In addition, we treat the opacity and emissivity for the remaining nearly 1.2 million 'secondary' b–b transitions in NLTE, if one level of a secondary transition is included in our detailed model.

Using this procedure to select our model atom, we obtain 13 675 primary Fe II NLTE lines between the 617 Fe II levels included in NLTE. For Fe II lines with $\lambda > 3500$ Å, we use 5–11 wavelength points within their profiles. In extensive test calculations, we have found that Fe II lines with $\lambda < 3500$ Å do not require these additional wavelength points in their profiles, due to the fine wavelength grid used in the model calculations at these wavelengths (Hauschildt & Baron 1995). This procedure typically leads to about 30 000 wavelength points for the model iteration and the synthetic spectrum calculations. Fig. 2 illustrates the adequacy of this procedure. We compare the output spectra of two models, which were iterated independently: one has the line-by-line opacity sampling below 3500 Å and the other has full line profiles for all NLTE lines. Clearly this wavelength grid is sufficiently dense for the calculations. This is mostly due to the properties of the Fe II ion, in particular the fact that its lines are concentrated mostly in the wavelength range below 3500 Å. Other model atoms, e.g. Ti I, require additional wavelength points for practically every line (Hauschildt et al., in preparation). For all primary lines, the radiative rates and the 'approximate rate operators' (see Hauschildt 1993) are computed and included in the iteration process. A detailed description of the Fe II line treatment is presented in Hauschildt et al. (1996).

4 RESULTS

In this section we compare and contrast the effects of NLTE Fe II in SNe II, in which iron is only a trace element, with those in SNe Ia, in which iron is a major constituent. We will discuss the transition class SNe Ib/c in future work. Table 1 describes the basic model parameters for the spectra that we use to illustrate the NLTE effects.

4.1 SNe II

In SNe II, iron is only a trace element in the outer ejecta, and thus one might expect that its effects on spectrum formation would be small. This is not the case, since iron line blanketing still plays the dominant role in the formation of the spectrum. Figs 3 and 4 display calculations with Fe II treated in LTE and NLTE compared to observed spectra of SN 1987 A 13 and 31 days after explosion. The varying role

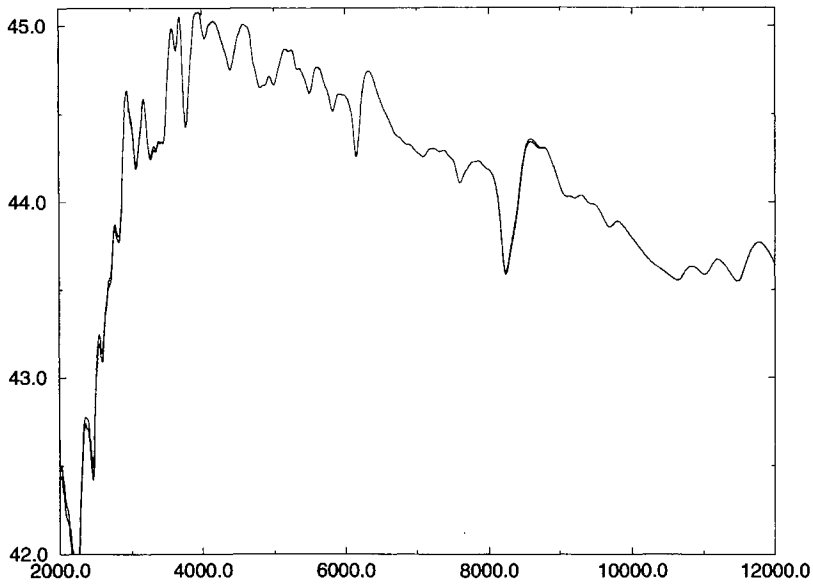

Figure 2. The solid line shows the result of a calculation of an SN Type Ia model with every line profile function included with 5 points per line, for a total of 83 269 wavelength points; the dashed line shows the result of sampling for $\lambda < 3500$ Å, with a total of 38 465 wavelength points.

Table 1. Parameters of presented models.

Model	$T_{\rm model}$	R_0	v_0	$X_{\rm Ni}$	Abund	N	v_e
SN 87A_day_13	5400	6.1×10^{14} cm	5500 km s^{-1}	0.03	$0.33\,Z_\odot$	6	—
SN 87A_day_13	5100	4.5×10^{14} cm	1700 km s^{-1}	0.01	$0.4\,Z_\odot$	6	—
SN Ia	9000	9.7×10^{14} cm	7500 km s^{-1}	0.05	W7	—	900 km s^{-1}

The basic model parameters for the spectra presented. The model atmospheres are characterized by the following parameters (see Hauschildt et al. 1992 and Baron et al. 1995 for details): the model temperature $T_{\rm model}$, which is defined by means of the luminosity, L, and the reference radius, R_0 [$T_{\rm model} = (L/4\pi R_0^2\sigma)^{1/4}$ where σ is Stefan's constant]; the reference radius R, which is the radius at which the continuum optical depth in extinction at 5000 Å ($\tau_{\rm std}$) is unity; the expansion velocity, v_0, at the reference radius; the mass fraction of ^{56}Ni, $X_{\rm Ni}$, which is the source of non-thermal gamma-rays, the elemental abundances which are, for the SN 1987 A models, solar (Anders & Grevesse 1989) with metallicity scaled by the factor given in the table, and for the SN Ia model are W7 (Nomoto, Thielemann & Yokoi 1984) compositions, homogenized for $v > 8000$ km s^{-1}; and the density structure parameter, v_e, [$\rho(r) \propto \exp(-v/v_e)$], or [$\rho(r) \propto (v/v_0)^{-N}$].

of Fe II NLTE is nicely displayed in these figures. While we have attempted to fit the observed spectrum, neither the LTE nor NLTE models match the width of all of the observed features, since composition inhomogeneities as well as more complicated density structures (including clumping) are known to be important in SN 1987 A. Nevertheless, the NLTE Fe II models overall, particularly in the blue, provide a better fit to the observed spectra than do the LTE Fe II models.

In Fig. 3 the Hα and Hβ absorption is too narrow in both models, and the absorption feature at 5800 Å, which is likely due to He I λ 5876 and the Na D doublet, is poorly fit. However, below $\lambda \sim 4200$ Å, the NLTE model more closely follows the observed spectrum. In the later spectrum (Fig. 4), the overall fit of the NLTE model is again superior to that of the LTE spectrum, even though the Balmer lines are now quite complicated (probably because of composition inhomogeneities).

4.2 SNe Ia

In SNe Ia, where iron is a major constituent of the atmosphere, one would expect that Fe II NLTE effects would play a dominant role. Fig. 5a compares the results of two representative SNe Ia model calculations, where Fe II is treated in LTE and NLTE. In both cases the models have been iterated to radiative equilibrium. In order to better display the differences between the two calculations, Fig. 5b displays the differences between the two spectra, where a positive value implies more flux in the NLTE model. The differences are significant, particularly since one goal of spectral analysis through synthetic spectra is to determine abundances in supernovae.

Up to this point, when we have referred to LTE treatment, we have really meant transitions, for which the rates are not included in the solution of the rate equations. However, the source function is *not* treated in complete LTE in

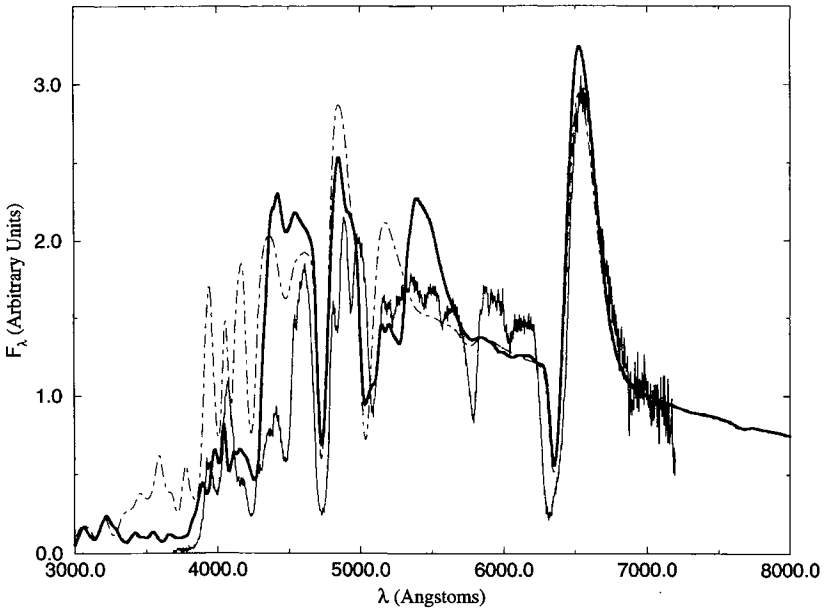

Figure 3. The observed spectrum of SN 1987 A (taken at CTIO) on 1987 March 8 (thin solid line) is compared to two model calculations with reference radii and velocities of 6.1×10^{14} cm and 5500 km s^{-1} and $T_{\rm model} = 5400$ K, $X_{\rm Ni} = 0.03$, and $Z = 0.33\ Z_\odot$. The density profile is a power law with $N = 6$ (model SN 87A_day_13 in Table 1). The thick solid line includes Fe II in NLTE, whereas the thin dot-dashed line displays a calculation in which Fe II is treated in LTE.

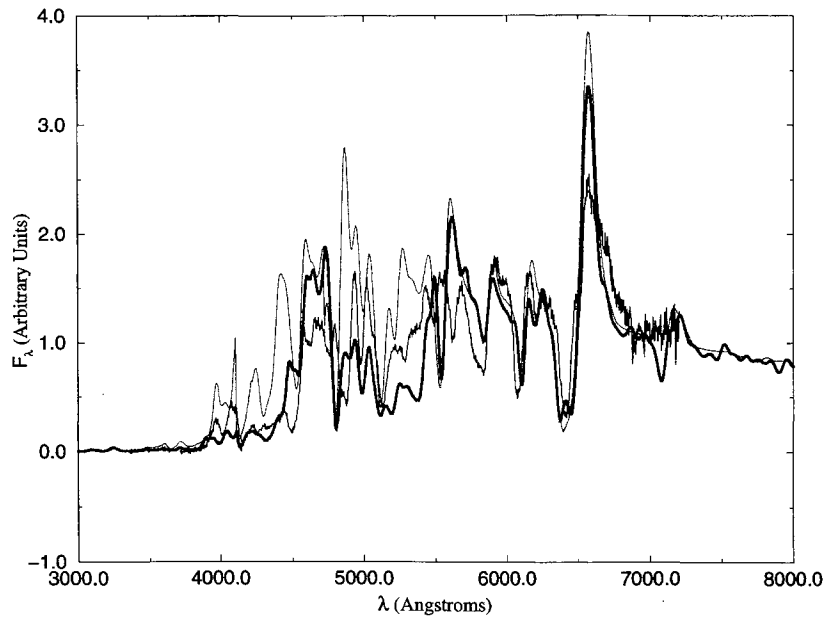

Figure 4. The observed spectrum of SN 1987 A (taken at at CTIO) on 1987 March 26 (thin solid line) is compared to two model calculations with reference radii and velocities of 4.5×10^{14} cm and 1700 km s^{-1} and $T_{\rm model} = 5100$ K, $X_{\rm Ni} = 0.01$, and $Z = 0.4\ Z_\odot$. The density profile is a power law with $N = 6$ (model SN 87A_day_31 in Table 1). The thick solid line includes Fe II in NLTE, whereas the thin dot-dashed line displays a calculation in which Fe II is treated in LTE.

that we write the source function in the line as:

$$S_\lambda = \varepsilon B_\lambda + (1-\varepsilon) J_\lambda,$$

where ε is the thermalization parameter (which we take to be a constant in the range $0.05 \leq \varepsilon \leq 0.1$) and the other symbols have their usual meaning. In a pure LTE treatment $\varepsilon = 1$, and in a 'pure scattering' treatment $\varepsilon = 0$. Fig. 6 compares the results of a full NLTE treatment, a pure LTE treatment, and a pure scattering treatment of the lines, with the structure held fixed. The results are quite interesting. The pure LTE case reproduces the overall spectral shape of the NLTE case rather well, while the pure scattering case does not. In fact the overall luminosity differs, between the NLTE case and the pure scattering case, by more than a factor of 2. The lineshapes, however, are better reproduced in the pure scattering case. This result is not surprising,

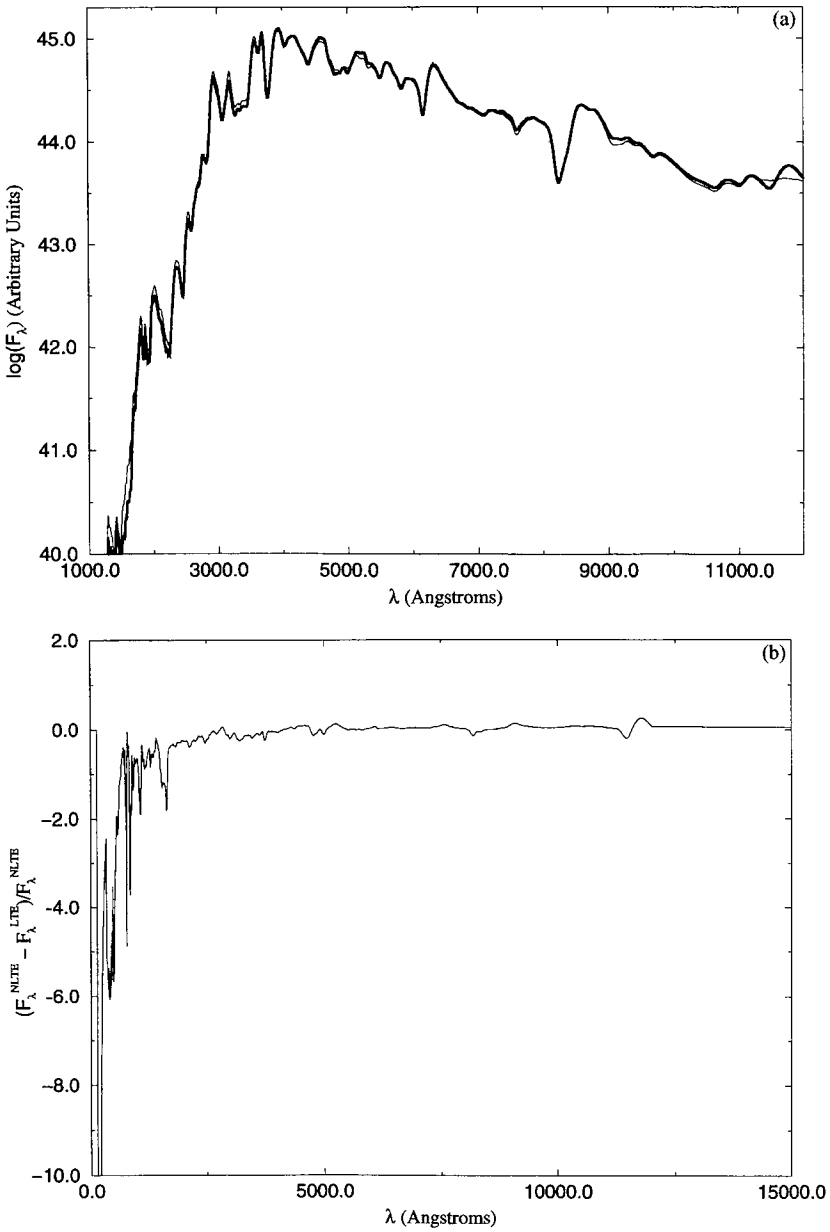

Figure 5. In panel (a) the thick solid line corresponds to a SN Ia model in which Fe II is treated in NLTE, and the thin solid line corresponds to a model in which Fe II is treated in LTE. Both models are iterated to radiative equilibrium and have the parameters: W7 (Nomoto, Thielemann, & Yokoi 1984) compositions, homogenized for $v > 8000$ km s^{-1}, reference radii and velocities of 9.7×10^{14} cm and 7500 km s^{-1} and $T_{\rm model} = 9000$ K, $X_{\rm Ni} = 0.05$ (model SN Ia in Table 1). The density profile is an exponential in velocity with scale $v_e = 900$ km s^{-1}. The thick solid line includes Fe II in NLTE, whereas the thin dot-dashed line displays a calculation in which Fe II is treated in LTE. Panel (b) shows the relative difference between the spectra shown in panel (a), where a positive value corresponds to more flux in the NLTE model.

since in many lines an analytic estimate of ε, such as is given by the equivalent two-level atom formulation, would predict a very small value of $\varepsilon \lesssim 0.01$. On the other hand, the total shape of the spectrum depends on the interaction between lines and continua as well as the interaction between overlapping lines (i.e. blanketing, blending, and collisions in the multiplets). The dotted line shows a case in which only 594 b–b transitions have been included, and illustrates that the 'pure scattering' approximation does not correctly pass flux from blue to red. Thus, even though it reproduces the line-shapes in the optical, and since it has the opacity to correctly reduce the flux due to line blending, the flux is simply scattered and is not passed to longer wavelengths as it should be. In the NLTE case, the multitude of collisions within multiplets (see also Höflich et al. 1996) creates a pseudo-thermal pool of photons which are in equilibrium among themselves and have a more nearly isotropic momentum distribution.

4.3 NLTE effects on the Fe II ionization

In Fig. 7 we display the ground state departure coefficients, b_1, for two supernova models. Since SNe produce significant amounts of radioactive ^{56}Ni, it is important to include the

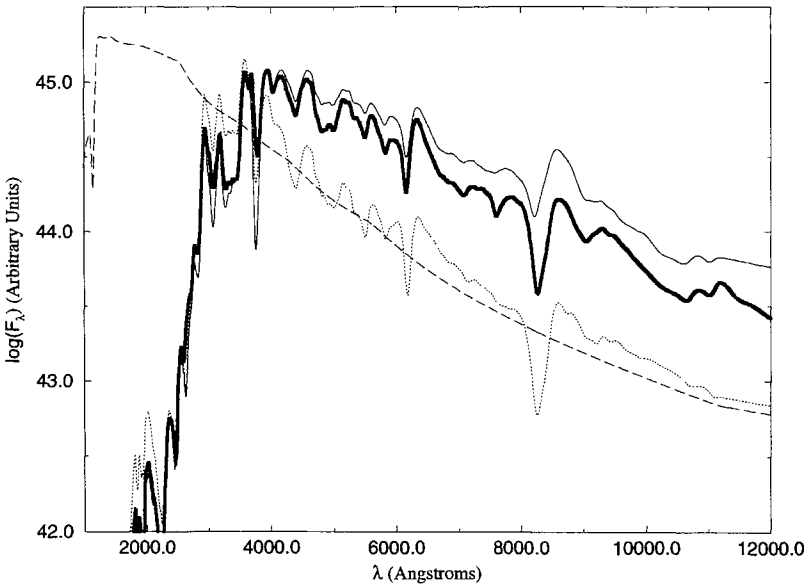

Figure 6. The results of a model calculation in which the lines are treated in full NLTE (thick solid), in pure LTE (thin solid), in pure scattering (short-dashed), and where only the 594 b–b transitions of the model atoms Mg II, Ca II, O I, Na I, Ne I, H I, He I, and He II, are included (long-dashed line).

effects of non-thermal electron (produced by γ-ray deposition) collisions in the NLTE rate equations. In the models presented here, the γ-ray deposition is treated as local due to a nickel mass fraction X_{Ni}, described in Table 1. The effects of non-thermal collisional ionization by primary electrons, produced by collisions with gamma rays due to the decay of ^{56}Ni and ^{56}Co, are modelled using the continuous slowing-down approximation (Garvey & Green 1976; Swartz 1991; Baron et al. 1996b). We have also included ionizations due to secondary electrons (Swartz 1991; Baron et al. 1996b), but most of their energy is thermalized and therefore has only a small effect on the level populations (Meyerott 1980). The collisional cross-sections are taken from the work of Lotz (1967a,b, 1968a,b,c).

Figs 7 (a) and (b) show the results for the model SN Ia with and without non-thermal effects, whereas Figs 7 (c) and (d) show the results for the model SN 87 A_day_13, with and without non-thermal effects. We have marked the b_1 for Fe II with connected plus signs for clarity. In all models, the departures from LTE are significant. In most regions of the supernova atmospheres, the Fe II b_1 are smaller than unity. This usually indicates an over ionization of Fe II relative to LTE, but we will see below that this is not always the case. The departure coefficients of other species show the same behaviour as Fe II, which is very different from the results we have obtained in our nova atmosphere modelling (Hauschildt et al. 1996). The sharp drop of the departure coefficients of He I in the model SN 87 A_day_13 is caused by the ionization of helium by non-thermal electrons in this model, as can be seen by comparing the models with and without non-thermal effects. Most affected by the non-thermal effects are He I, Fe II, and Mg II. Ca II appears to be hardly affected. Comparing the SN Ia models with and without non-thermal effects, it is evident that the non-thermal effects play an important role in determining the level populations. Again, Ca II appears to be the least affected by non-thermal effects. In the SN II model, O I is not strongly affected by non-thermal collisions, although that is not the case in the SN Ia model. In the SN Ia model, NLTE effects are quite small when non-thermal ionization is neglected. This may be due to the fact that since SN Ia atmospheres consist entirely of metals, with lower ionization energies than hydrogen and helium, thermal electron collisions act to restore LTE. Once all important non-thermal electron collisions are included, NLTE effects become important.

In Fig. 8 we display the ionization structure of iron throughout the atmosphere for model SN 87 A_day_13. Panels (a) and (b) show the NLTE results (with and without non-thermal electrons), whereas panels (c) and (d) show the results for LTE (but otherwise the same model structure). First we note the number of iron ionization stages that are present in the atmospheres (in a number of interleaved 'Strömgren spheres'). This is a more pronounced and well-known feature of nova atmospheres which is caused by the large temperature gradients inside the expanding shell. We find similar effects for all elements that are included in the model calculations.

The effects of NLTE on the Fe II ionization balance become clear by comparing panels (a) & (c) and (b) & (d) in Fig. 8. In the LTE case, Fe II is the dominant ionization stage of iron in the outer atmosphere. In the NLTE–Fe II case, however, Fe II recombines into Fe I throughout the outer atmosphere, although the ground state departure coefficients of Fe II are less than unity (the latter fact usually indicates an over-ionization relative to LTE). This is true whether or not non-thermal effects are included, although the iron remains ionized to lower optical depths when non-thermal effects are included. The reason for this non-intuitive ionization behaviour becomes clear when inspecting the graphs shown in Fig. 9. In the NLTE case (Fig. 9a), hydrogen remains ionized throughout the outer atmosphere, and the electron densities therefore remain high. However, in

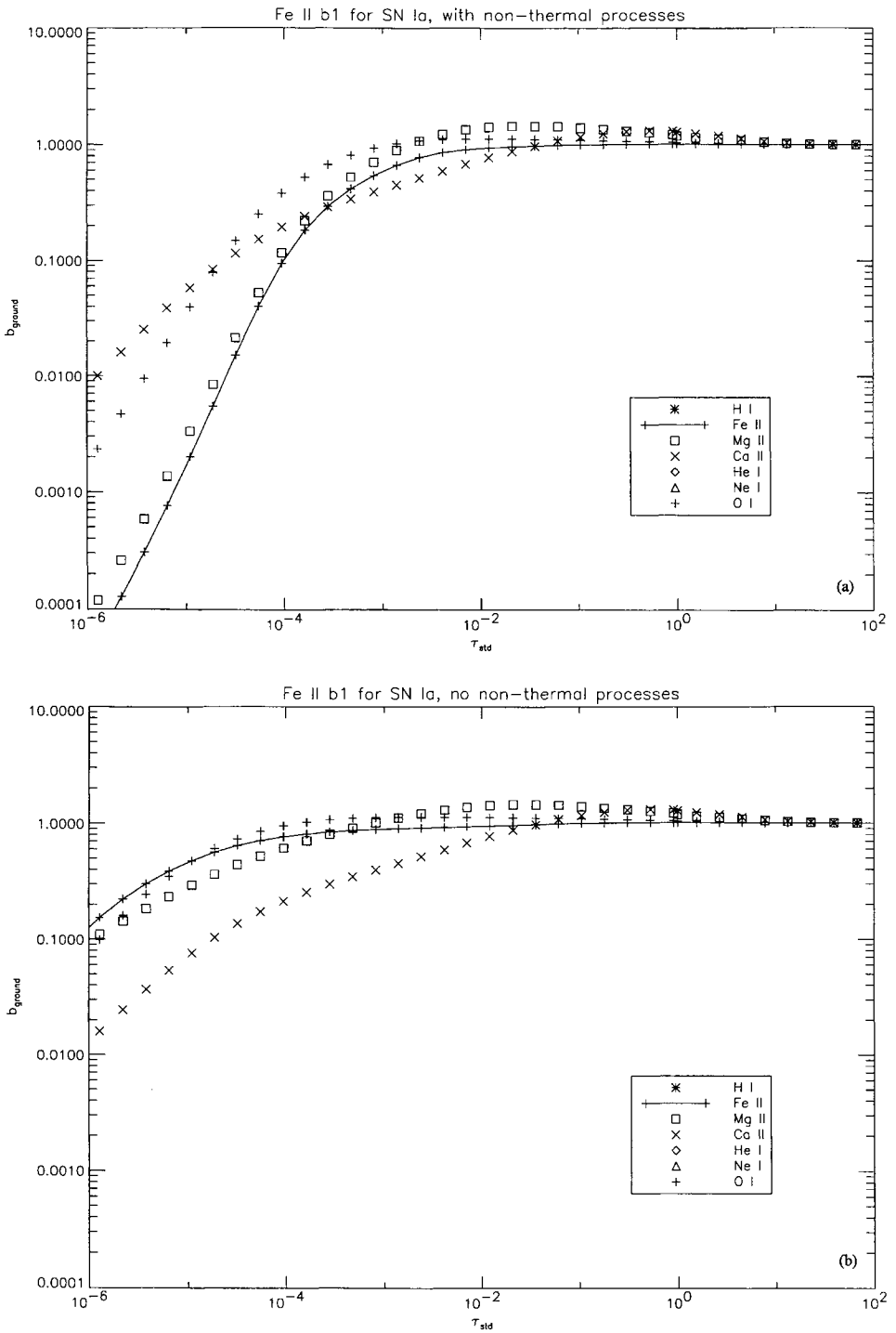

Figure 7. The run of the ground state departure coefficients b_1 for the NLTE species as functions of τ_{std} (the b–f optical depth at 5000 Å). Panels (a) and (b) show the results obtained for the model SN Ia, with and without non-thermal ionization, respectively; panels (c) and (d) show the model SN 87 A_day_13, with and without non-thermal ionization, respectively.

LTE, hydrogen recombines and the electron densities are much smaller than in the NLTE model. This completely changes the behaviour of the ionization equilibrium for *all* species, and the higher electron pressures combined with the different recombination rates in the NLTE model force the recombination of Fe II to neutral iron. This effect illustrates that NLTE modelling is extremely important, and must be done in great detail in order to obtain realistic results. In particular, this shows that fitting an observed SN II by using a model in LTE would force the choice of a high temperature in order to reproduce the Balmer lines. With this high temperature in LTE, the ionization of Fe could never be reproduced. The correlation of the recombination of iron with the ionization of hydrogen is evident upon

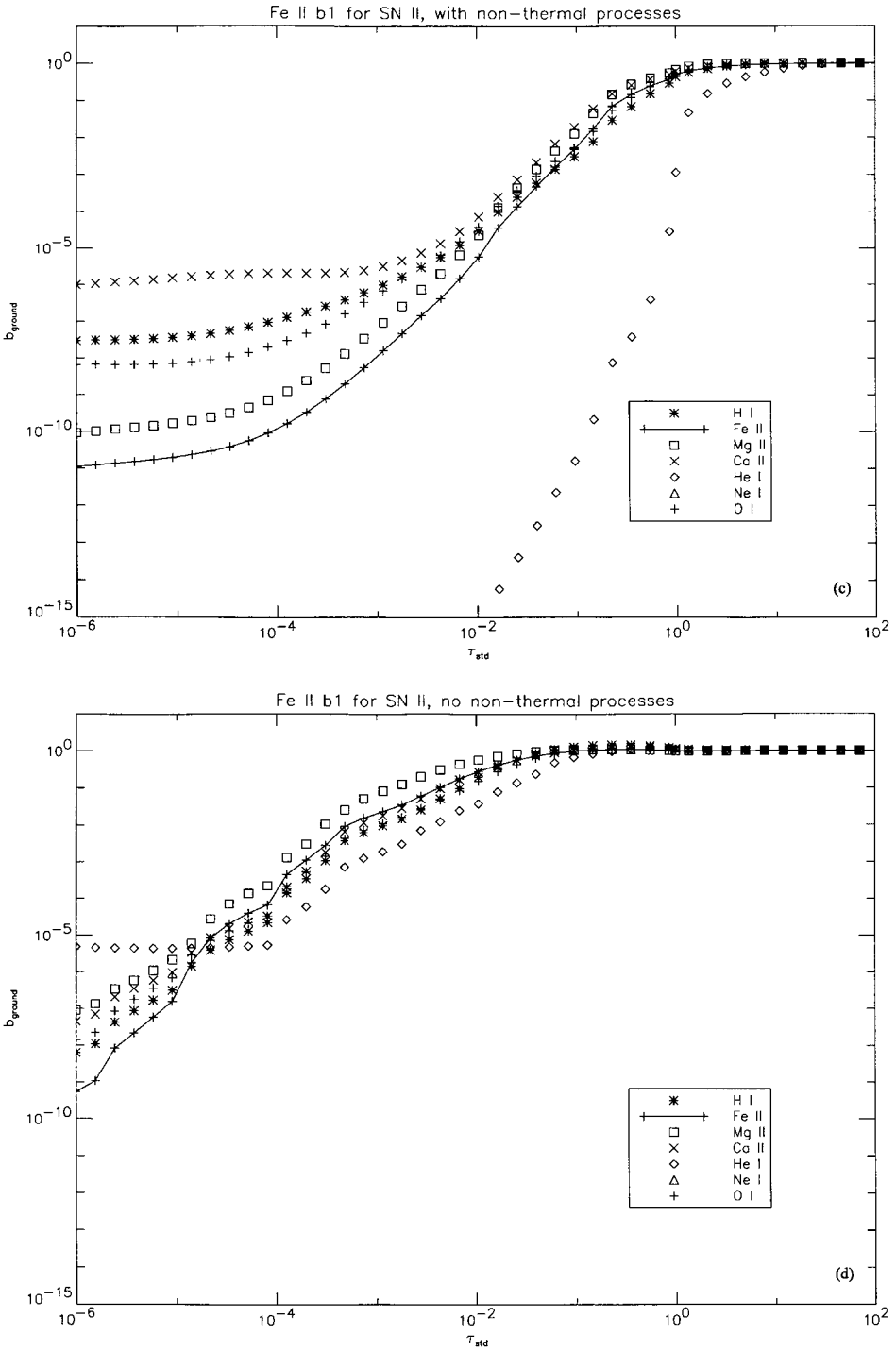

Figure 7 – *continued*

comparing Figs 9(a) and (c). In panel (a), which includes non-thermal electron collisions, the iron is neutral deeper into the atmosphere, whereas in panel (c), without non-thermal effects the iron is only recombining in the outer regions, just where the electron and H II fractions are rising.

In Fig. 10 we show that the changes in the iron ionization structure in the SN I model are very small. This is expected, since the ground state departure coefficients for Fe II are close to unity in this model. Again, with the neglect of non-thermal effects, the high electron fractions in SN Ia models drive them towards LTE. This is very different from the behaviour we find in both the SN II model and our nova model atmospheres (Hauschildt et al. 1996). The NLTE effects of Fe II in the SN I model will be apparent only in the line source functions and the spectra, as discussed below.

In Fig. 11 we show the departure coefficients for all the Fe II levels for the two models (with and without non-thermal effects) in an overview graph. This figure demonstrates

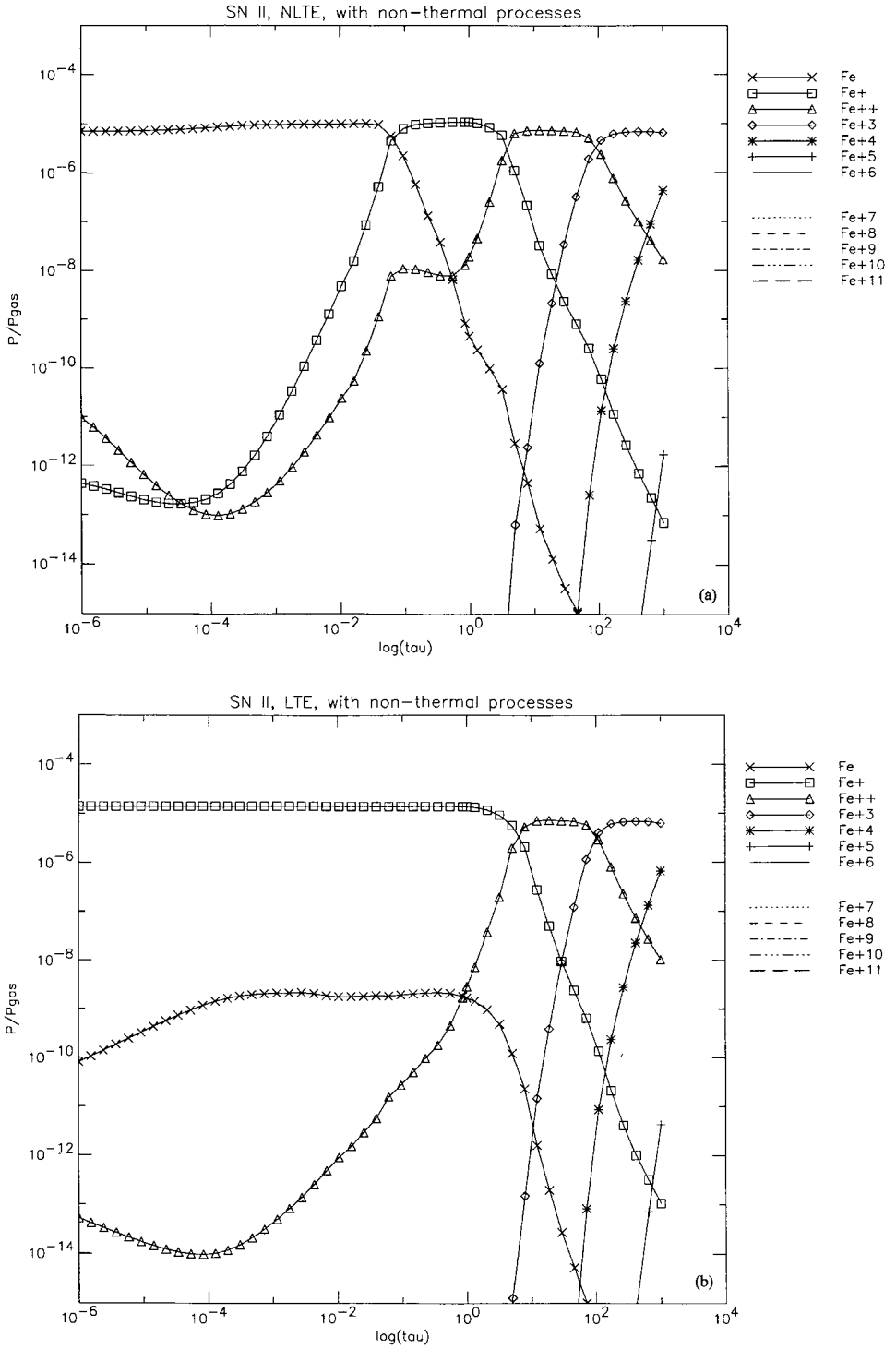

Figure 8. Ionization structure of iron as a function of τ_{std} (the b–f optical depth at 5000 Å) for the model SN 87 A_day_13. Panel (a) shows the results obtained with Fe II treated in NLTE, with non-thermal ionization; panel (b) shows NLTE without non-thermal ionization; panel (c) shows the results for LTE Fe II, with the structure of the non-thermally ionized model, and panel (d) shows LTE Fe II, with the structure of the model neglecting non-thermal ionization. The NLTE under-ionization causes Fe II to recombine to Fe I in the outer layers of the SN atmosphere. Note the number of 'Strömgren spheres' of various ionization stages of iron in the inner parts of the SN atmosphere.

that the NLTE effects for the Fe II are important, and differ for the individual levels and for different model temperatures (for a direct comparison of the effect of varying the model temperature in SNe II see Hauschildt & Baron 1995). For each T_{model}, the departure coefficients are closer to unity (their LTE value) for the higher-lying levels, which are more strongly coupled to the continuum than the lower-lying levels. The rather large variation of the b_i without the Fe II model atom suggests that the Fe II lines will show significant NLTE effects themselves, in addition to the

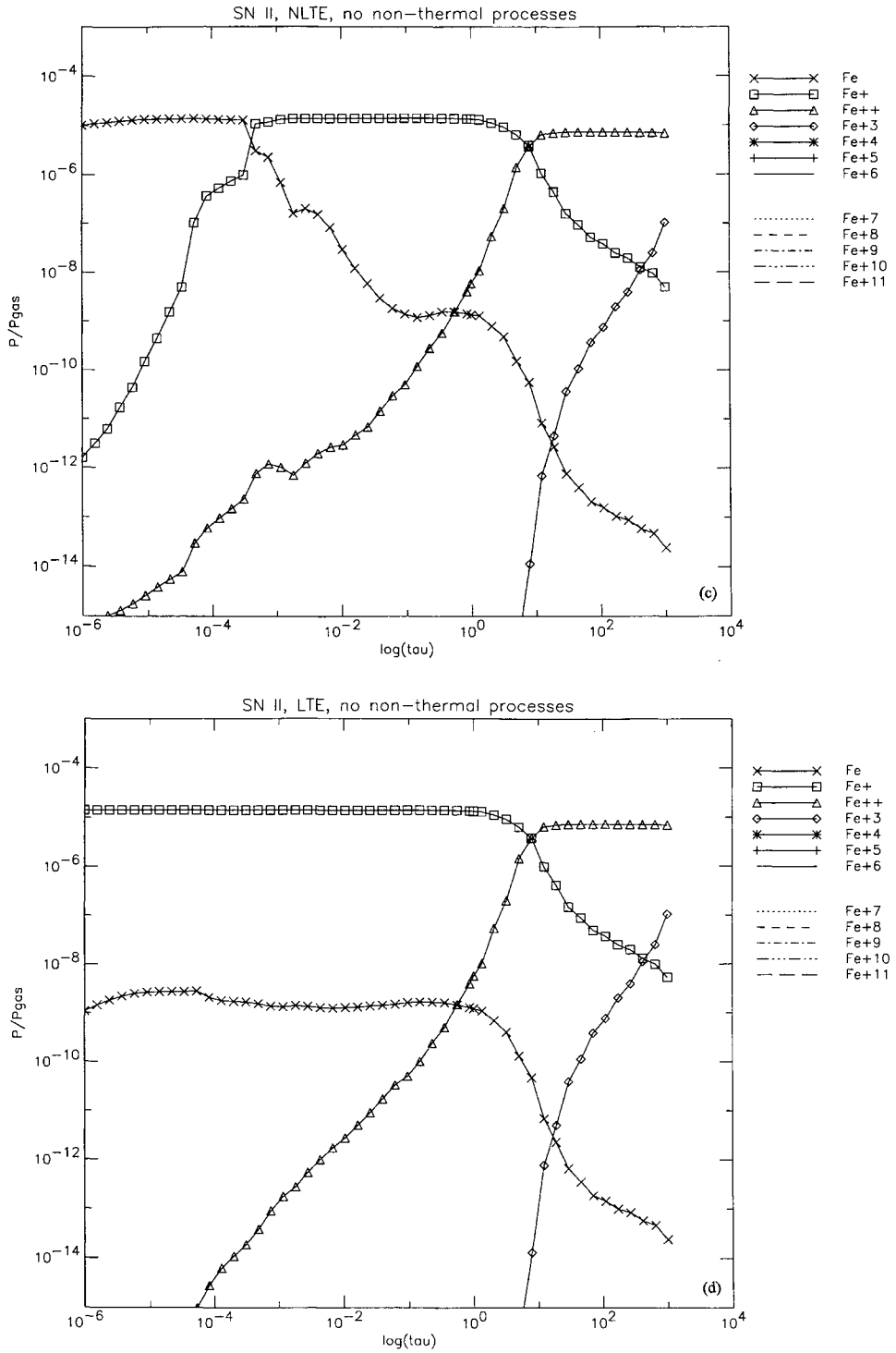

Figure 8 – *continued*

effects introduced by the changes in the ionization structure. Comparing the models with and without the non-thermal effects, we see that the models without non-thermal ionization have departure coefficients larger than unity at moderate optical depths; however, when non-thermal ionization is considered, the departure coefficients tend to stay below one.

4.4 NLTE effects on the formation of Fe II lines

The NLTE effects change not only the ionizations balance of iron but also the relative level populations of F II. We demonstrate this effect for two important Fe II multiplets. In Figs 12 (a) and (b) we show the ratio of the line source functions S_L to the local Planck function for the UV1 mul-

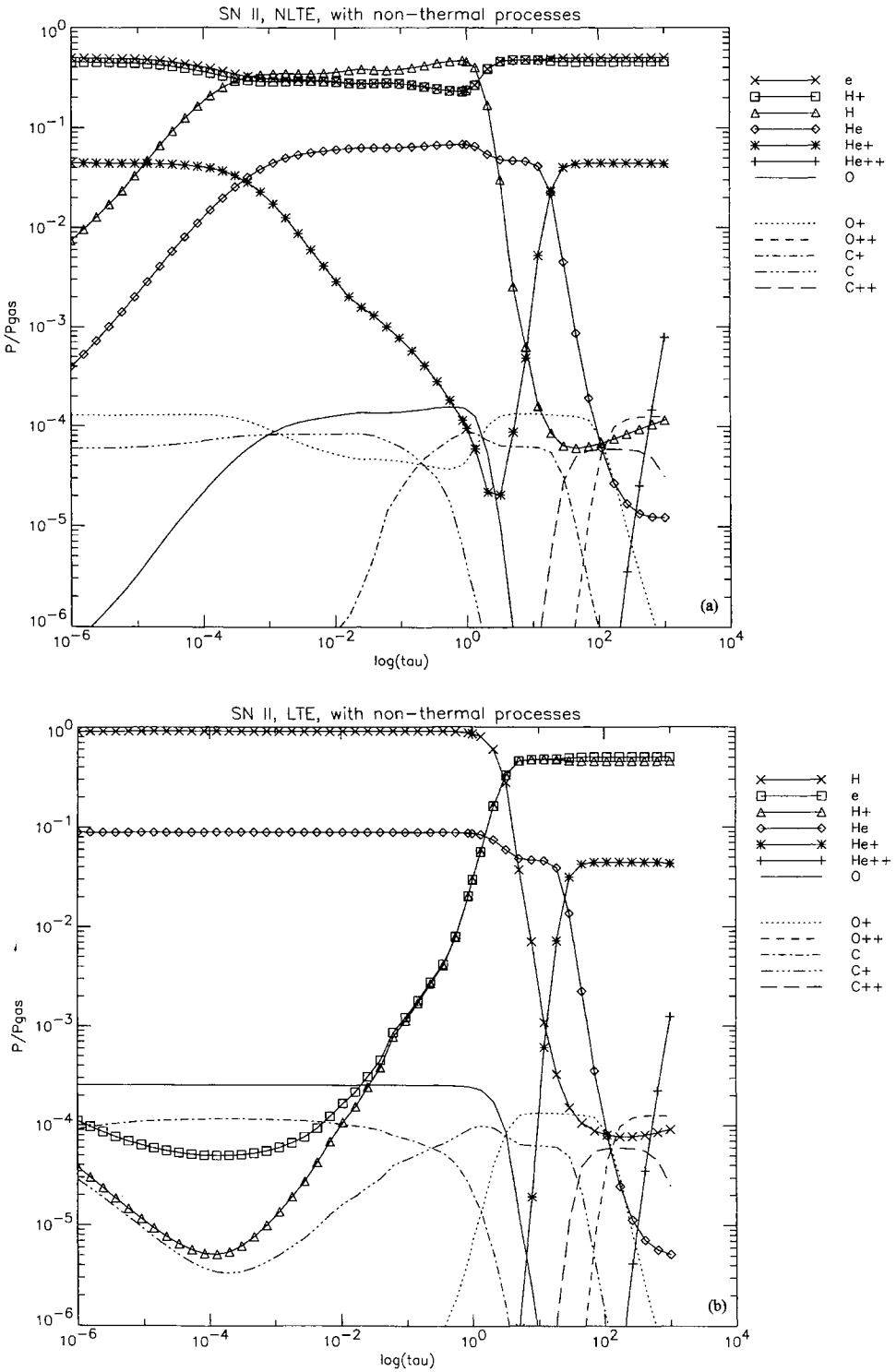

Figure 9. The concentrations of the most abundance species as functions of τ_{std} (the b–f optical depth at 5000 Å) for the model SN 87A_day_13. Panel (a) shows the results obtained within NLTE, including non-thermal ionization; panel (b) shows NLTE without non-thermal ionization, whereas panels (c) and (d) show the results for LTE, respectively. The NLTE under-ionization causes Fe II to recombine to Fe I in the outer layers of the SN atmosphere. Note the number of 'Strömgren spheres' of various ionization stages of iron in the inner parts of the SN atmosphere. Non-thermal processes prevent this recombination from occuring deeper in the atmosphere.

tiplet of Fe II. These are UV lines (around 2600 Å) from the ground a^6D term to the z^6D° term. In the model SN Ia which includes non-thermal effects (Fig. 12a, left panel), the UV1 multiplet is nearly in LTE up to the outer atmosphere. Only below $\tau_{std} = 10^{-3}$ do the line source functions differ, by about 20 per cent, from the Planck function. The situation is different for the model SN 87 A_day_13 (Fig. 12a, right panel). Here the line source functions are larger than the

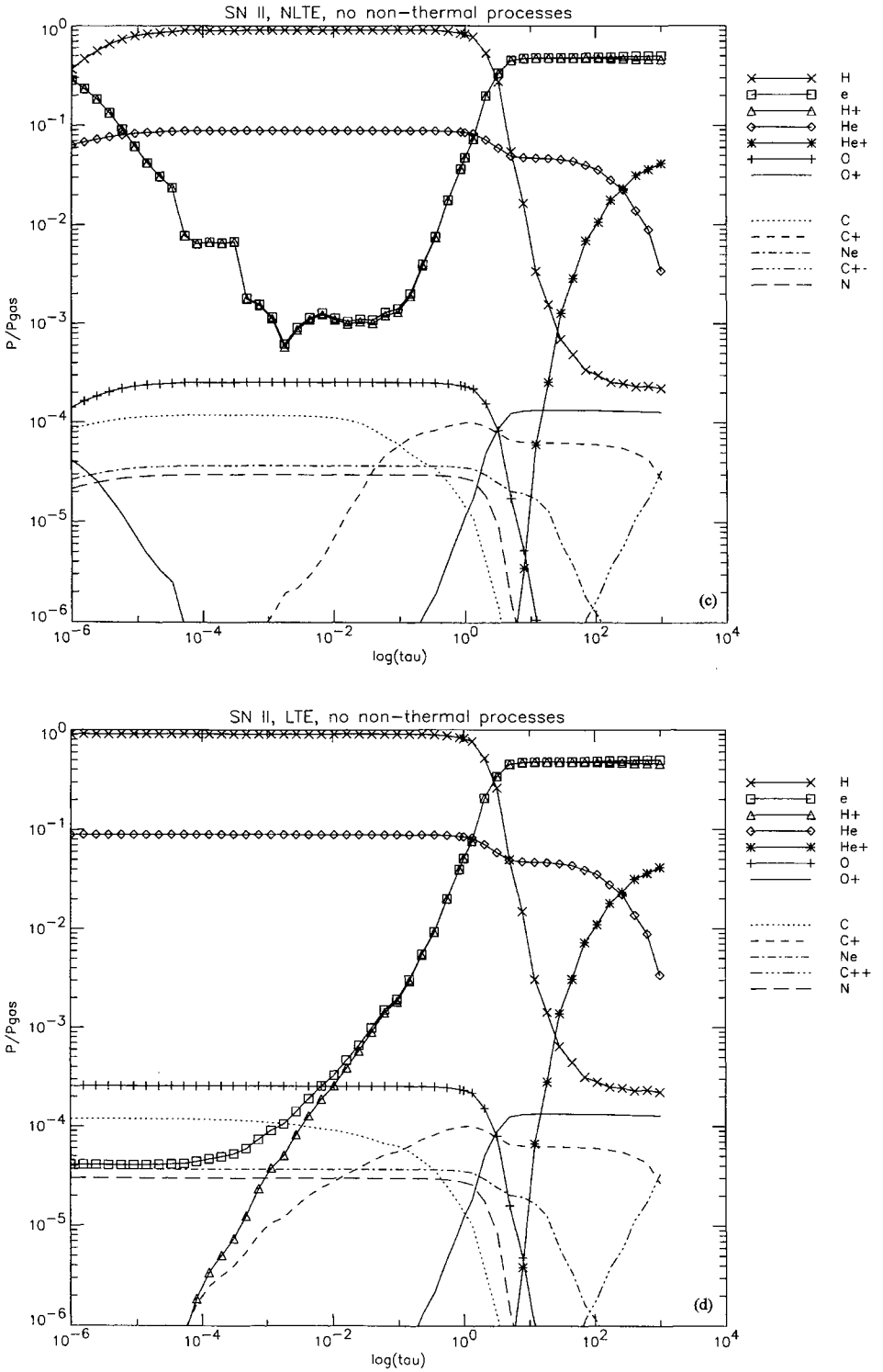

Figure 9 – *continued*

Planck function by nearly a factor of 2. In both models the (collisional) coupling between the levels of each term is strong enough to establish nearly the same line source function to Planck function, S_L/B, ratio for all lines within the multiplet, although the electron densities are relatively low. Only in the SN II model do the levels within a term finally decouple for $\tau_{\rm std} < 10^{-4}$. When non-thermal processes are neglected, the same general trend is observed, although now the SN II model has a UV1 line source function that is smaller than the local Planck function inside, but becomes greater than the local Planck function far out in the atmosphere.

The subordinate Fe II-multiplet 42 (a^6S to z^6P°) shows a somewhat different behaviour in Fig. 12a. The line source

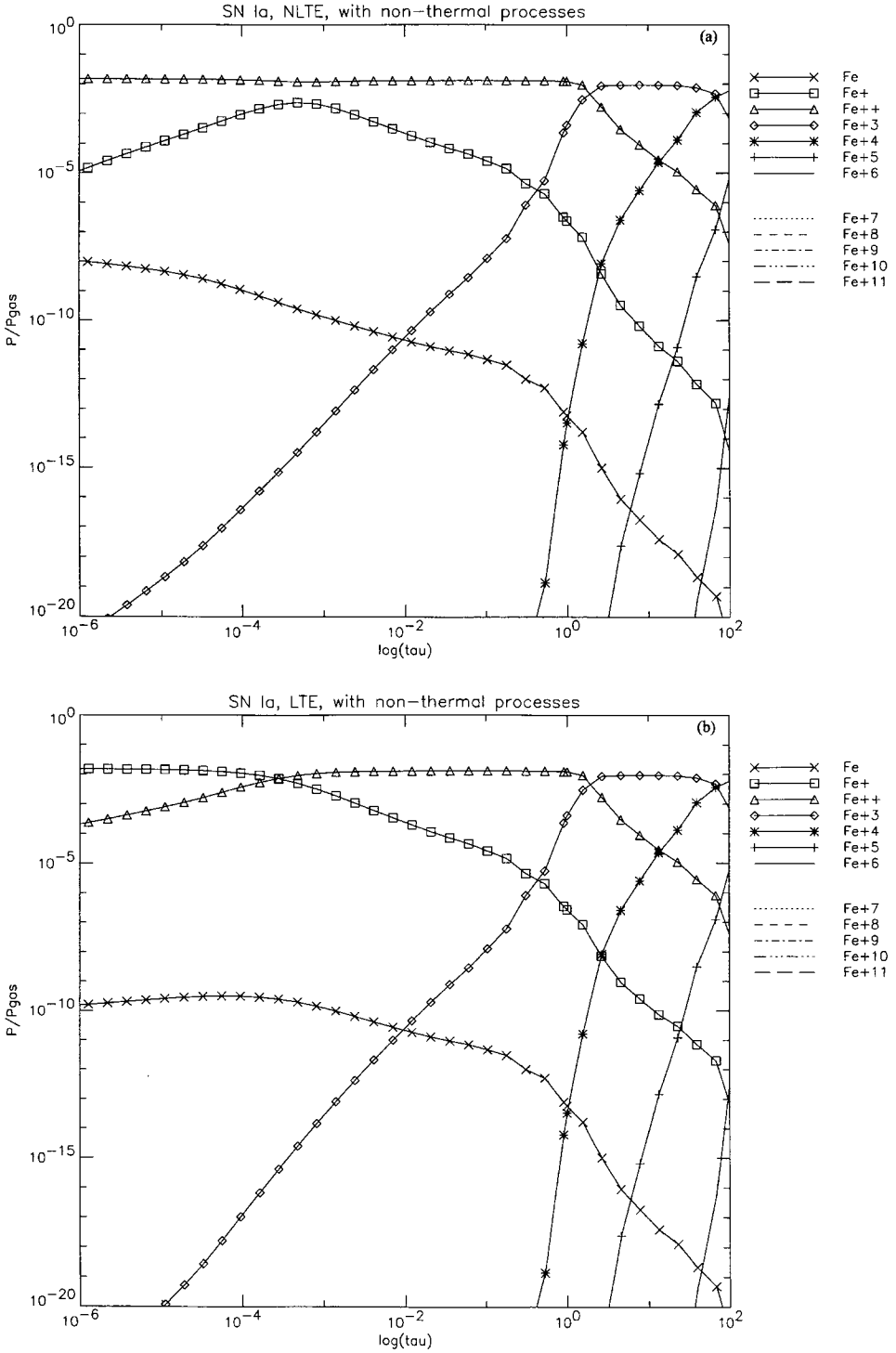

Figure 10. Ionization structure of iron as function of τ_{std} (the b–f optical depth at 5000 Å) for the model SN Ia. Panels (a) and (b) show the results obtained with Fe II treated in NLTE, with and without non-thermal ionization, respectively, whereas panels (c) and (d) show the results for LTE Fe II, with and without non-thermal ionization, respectively. In this model, the changes of the ionization of iron are very small and visible only in the outermost parts of the atmosphere. Note the number of 'Strömgren spheres' of various ionization stages of iron in the inner parts of the SN atmosphere.

functions for the three primary NLTE lines are slightly smaller than unity for $10^{-4} \leq \tau_{std} < 2$, and larger than unity for $\tau_{std} < 10^{-4}$ for the model SN Ia (left panel). The model SN 87 A_day_13 (right panel) shows nearly the opposite behaviour. The NLTE effects are slightly larger for the cooler model, as seen earlier for the UV1 multiplet. This shows that the NLTE effects for Fe II are not just over-ionization, but that the 'internal' NLTE effects are also significant. This multiplet is less affected by non-thermal ionization than is the UV1 multiplet.

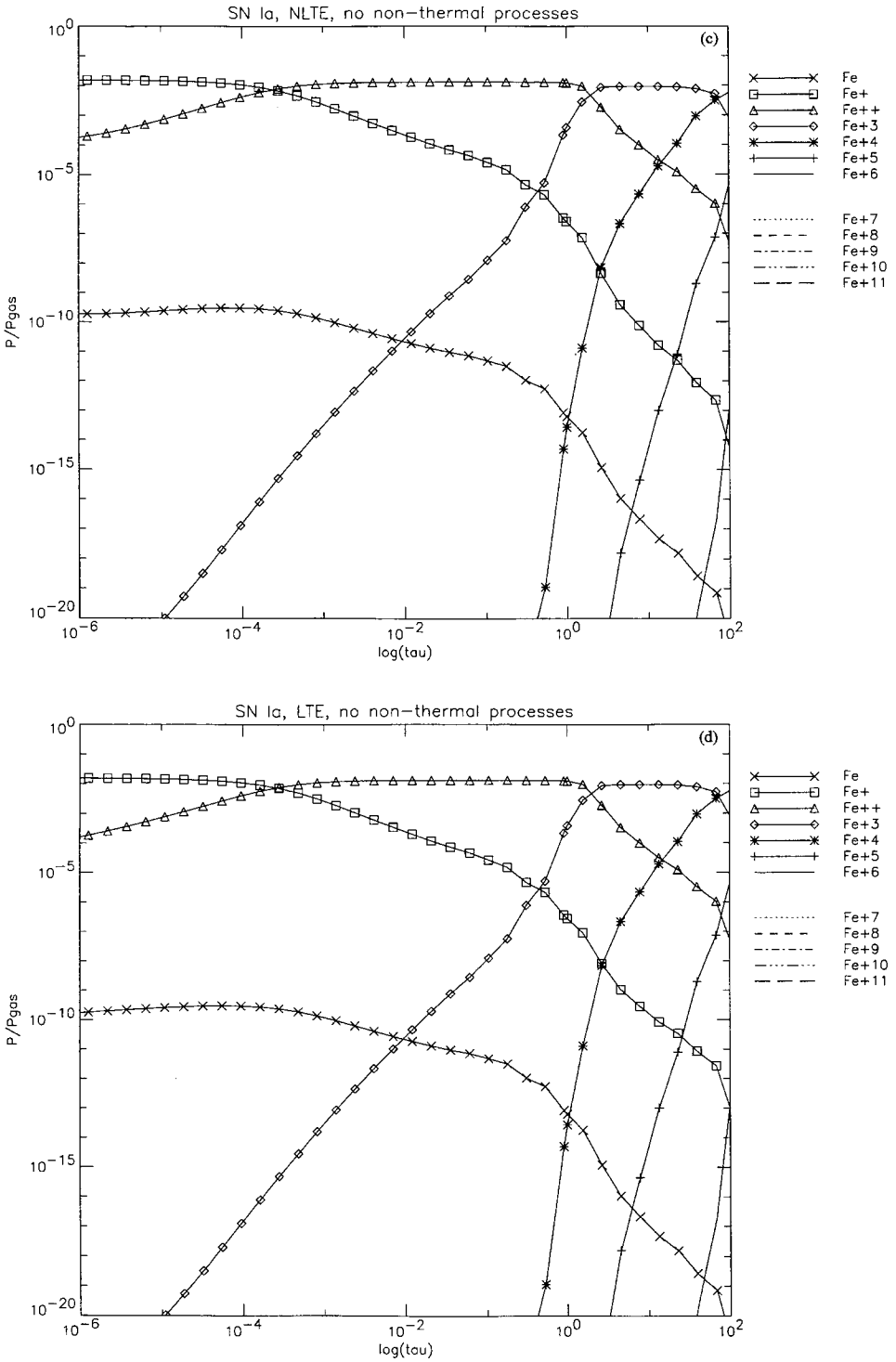

Figure 10 – *continued*

The Fe II NLTE effects we have found in SN I and II atmospheres are significantly *smaller* than in nova atmospheres (Hauschildt et al. 1996). This is due to the much higher velocity field in SN atmospheres, which tends to transfer photons from the regions neighbouring the Fe II lines into them, thus coupling the frequencies more strongly together than in the case of novae. This is also true for the regions around the ionization edges of Fe II, which limit the effective number of Fe II ionizing photons. It must be noted here that our departure coefficients, radiation field and source functions are *all* computed in the comoving frame and, therefore, simplified arguments based on Eulerian frame experience can and will lead to wrong conclusions. In the comoving frame, the velocity does *not* lead to a frequency shift of the photons (by its construction), but leads instead to terms which are better described as 'drag' terms,

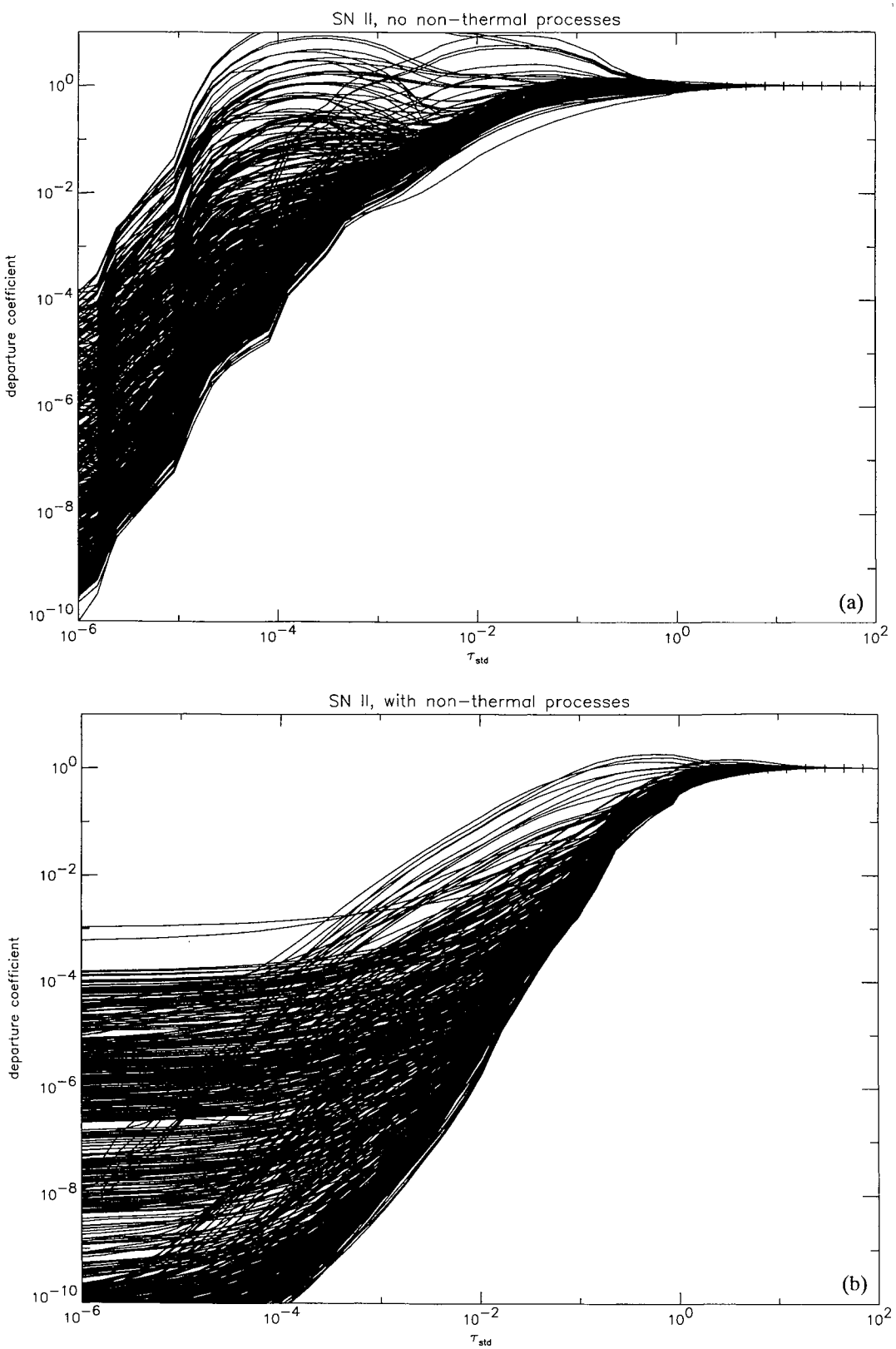

Figure 11. The departure coefficients for all NLTE levels of Fe II as functions of the standard optical depth τ_{std} for two models: SN Ia, with and without non-thermal effects [panels (a) and (b)] and SN 87 A_day_13, with and without non-thermal effects [panels (c) and (d)]. The departure coefficients are closer to unity for the higher-lying levels.

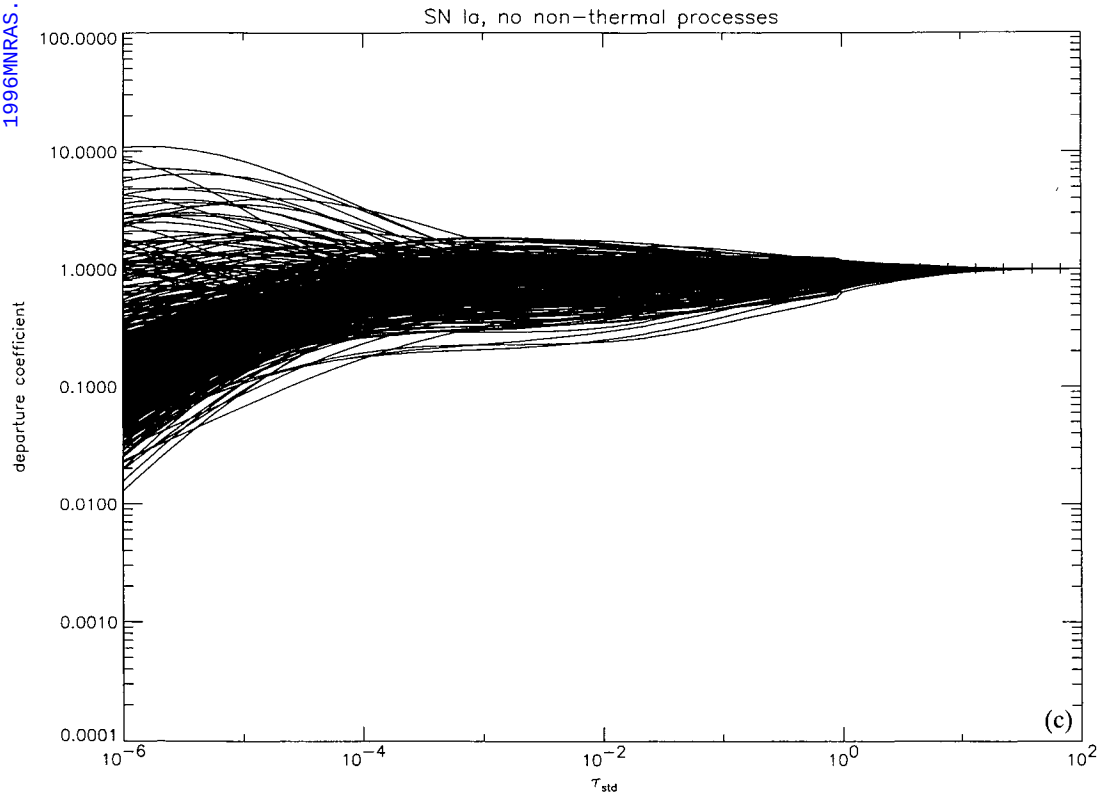

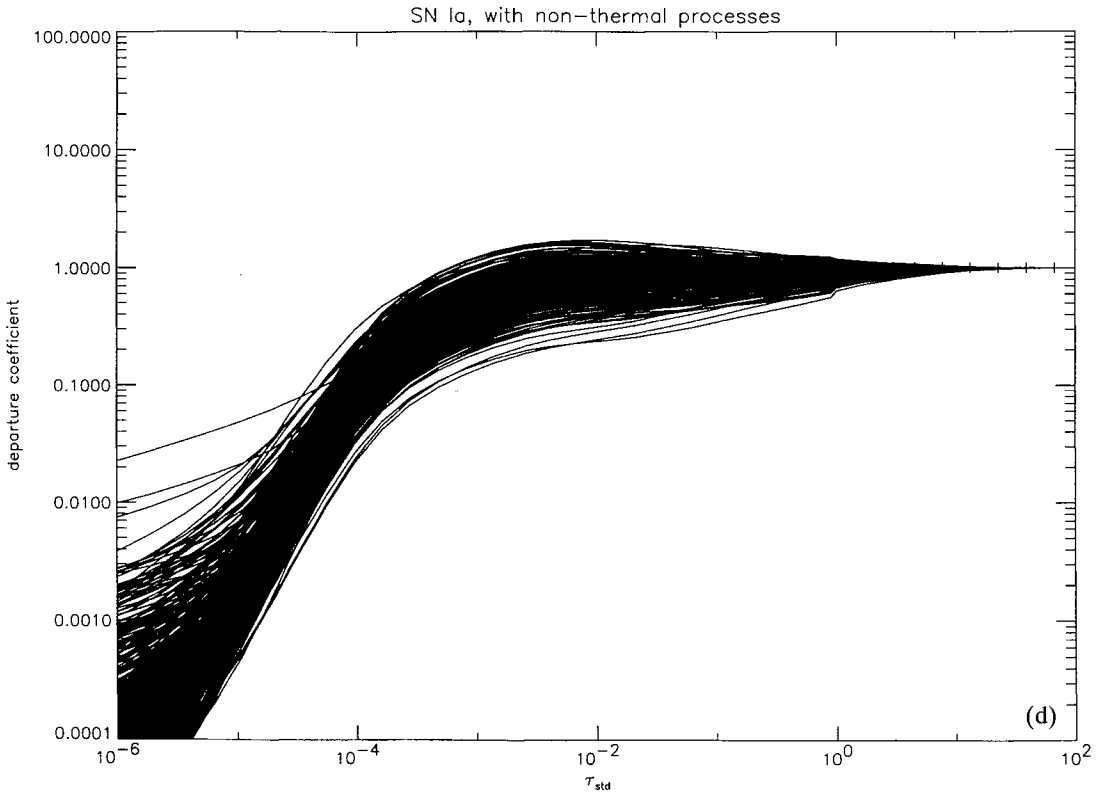

Figure 11 – *continued*

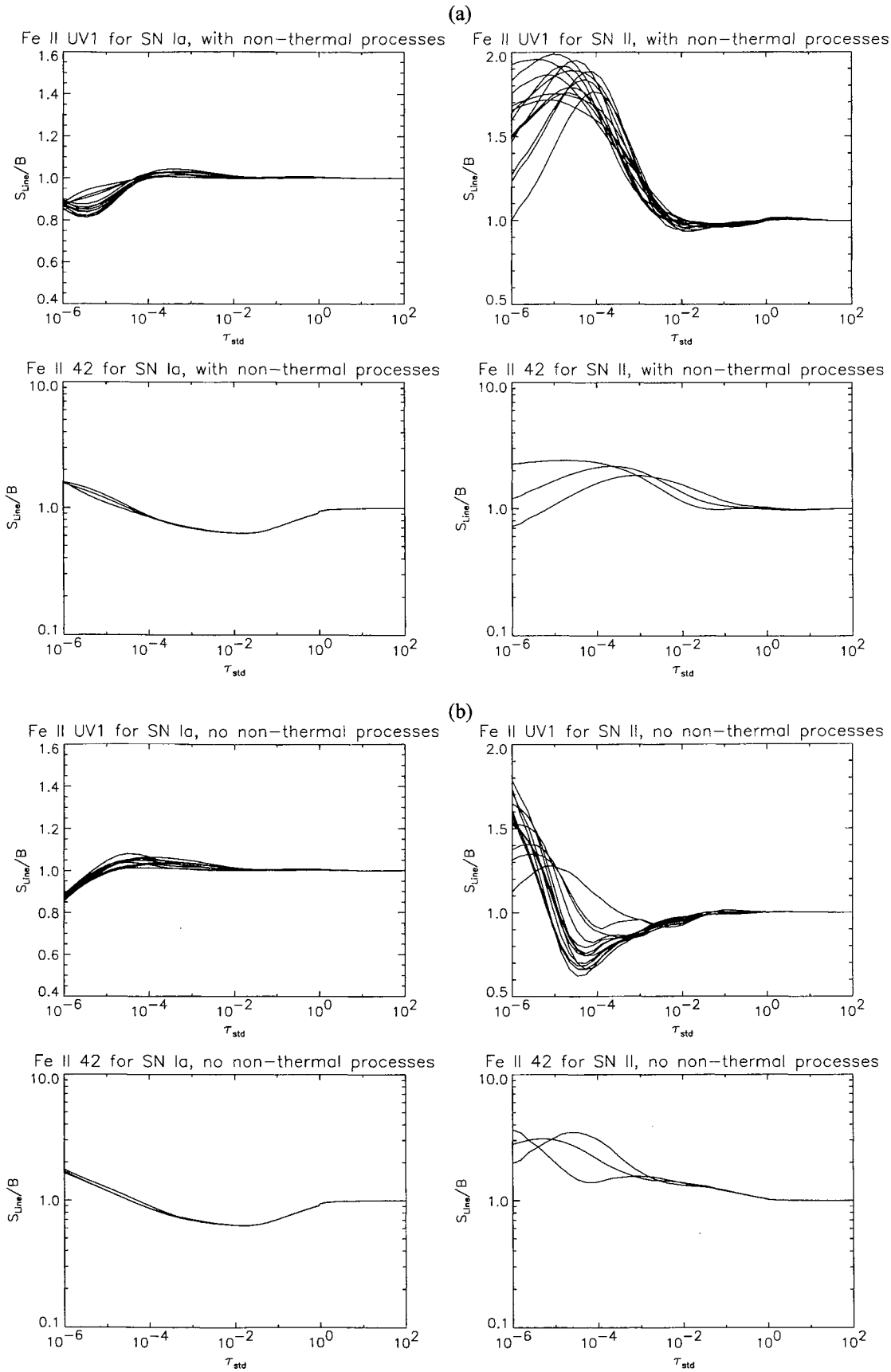

Figure 12. The ratio of the line source function to the local Planck function for the UV1 multiplet (a^6D to z^6D^0) and the multiplet 42 (a^6S to z^6P^0) as functions of the standard optical depth. The left side displays the model SN Ia and the right side the model SN 87 A_day_13. Panel (a) includes non-thermal ionization and panel (b) does not.

slowing the response of the radiation field to changes in the opacity as a function of wavelength when compared to the static case. This 'stiffer' radiation field limits the magnitude of the NLTE effects on the line formation; in fact, this is more effective at higher velocities. Therefore, stellar winds and novae show comparatively larger NLTE effects than the very rapidly expanding atmospheres of SNe.

5 CONCLUSIONS

We have demonstrated that large model atoms are required in order to correctly transport energy and push the flux from blue to red in SNe atmospheres. Weak lines must be included in order to correctly reproduce line blanketing and blending. In spite of the fact that an equivalent two-level atom approach would predict very small values of the thermalization parameter ε for many transitions, collisions in the multiplets and continuum effects redistribute the energy and momentum such that an overall higher value of ε leads to a more accurate description of the radiation transport. A calculation that treats weak lines as pure scattering misses far too much opacity and gives results similar to those that treat only continua. Accurate modelling of the UV also requires large model atoms and the inclusion of weak lines as background opacity. As better atomic data become available, the accuracy of the calculations should improve. NLTE effects cause very non-intuitive ionization effects to occur, which show that these effects must be included in detail.

ACKNOWLEDGMENTS

We thank the referee for suggestions which improved the presentation of this paper. This work was supported in part by NASA grants NAGW-4510, NAGW-2628 and NAGW 5-3067 to Arizona State University; NSF grants AST-9417242 and AST-9115061; and an IBM SUR grant to the University of Oklahoma. Some of the calculations presented in this paper were performed at the Cornell Theory Center (CTC) and at the San Diego Supercomputer Center (SDSC), supported by the NSF, and at the National Energy Research Supercomputer Center (NERSC), supported by the U.S. DoE. We thank them for a generous allocation of computer time.

REFERENCES

Anders E., Grevesse N., 1989, Geochim. Cosmochim. Acta, 53, 197
Baron E. et al., 1995, ApJ, 441, 170
Baron E., Hauschildt P. H., Mezzacappa A., 1996a, MNRAS, 278, 763
Baron E., Hauschildt P. H., Branch D., Kirshner R. P., Filippenko A. V., 1996b, MNRAS, 279, 779
Eastman R., Pinto P., 1993, ApJ, 412, 731
Garvey R. H., Green A. E. S., 1976, Phys. Rev. A, 14, 946
Hauschildt P. H., 1992, J. Quant. Spectrosc. Radiat. Transfer, 47, 433
Hauschildt P. H., 1993, J. Quant. Spectrosc. Radiat. Transfer, 50, 301
Hauschildt P. H., Baron E., 1995, J. Quant. Spectrosc. Radiat. Transfer, 54, 987
Hauschildt P. H., Wehrse R., Starrfield S., Shaviv G., 1992, ApJ, 393, 307
Hauschildt P. H., Störzer H., Baron E., 1994, J. Quant. Spectrosc. Radiat. Transfer, 51, 875
Hauschildt P. H., Starrfield S., Shore S. N., Allard F., Baron E., 1995, ApJ, 447, 829
Hauschildt P. H., Baron E., Starrfield S., Allard F., 1996, ApJ, 462, 386
Höflich P., 1995, ApJ, 443, 89
Höflich P., Khokhlov A., Wheeler J. C., Nomoto K., Thielemann F.-K., 1996, in Canal R., Ruiz-Lapuente R., Isern J., eds, NATO ASI Conference on Thermonuclear Supernovae. Kluwer, Dordrecht
Kurucz R., 1994, CDROM No. 22: Atomic Data for Fe, Co, and Ni. SAO Cambridge, MA
Lotz W., 1967a, ApJS, 14, 207
Lotz W., 1967b, Journal Opt. Soc. America, 57, 873
Lotz W., 1968a, Journal Opt. Soc. America, 58, 236
Lotz W., 1968b, Journal Opt. Soc. America, 58, 915
Lotz W., 1968c, Z. Physik, 216, 241
Meyerott R. E., 1980, ApJ, 239, 257
Mihalas D., Mihalas B. W., 1984, Foundations of Radiation Hydrodynamics. Oxford Univ. Press, Oxford
Nomoto K., Thielemann F.-K., Yokoi K., 1984, ApJ, 286, 644
Nugent P., Baron E., Hauschildt P., Branch D., 1995, ApJ, 441, L33
Peraiah A., 1987, ApJ, 317, 271
Peraiah A., 1991a, ApJ, 371, 673
Peraiah A., 1991b, ApJ, 380, 212
Swartz D., 1991, ApJ, 373, 604